Astron. Astrophys. 233, 207–219 (1990)

ASTRONOMY AND ASTROPHYSICS

Flow patterns in a sunspot region observed in the photosphere, chromosphere and transition region

K.P. Dere [1], B. Schmieder [2], and C.E. Alissandrakis [3]

[1] E.O. Hulburt Center for Space Research, U.S. Naval Research Laboratory, Washington, DC 20375-5000, USA
[2] Observatoire de Paris, Section de Meudon, DASOP, F-92195 Meudon Principal Cedex, France
[3] Section of Astrophysics, Astronomy and Mechanics, Department of Physics, University of Athens, GR-15783 Athens, Greece

Received October 4, accepted November 27, 1989

Abstract. During the Spacelab 2 mission, the sunspot in NOAA-AR 4682 was the object of a coordinated observing campaign that included the ultraviolet HRTS spectrograph on Spacelab 2 and the ground-based instruments at the Meudon Observatory: the spectroheliograph, the magnetograph, and the Multichannel Subtractive Double Pass Spectrograph (MSDP). The analysis of the data in this paper has concentrated on understanding the large scale Evershed flow in the photosphere (Fe I 6173 Å), chromosphere (H$\alpha \pm 0.3$ Å) and the transition region (C IV 1548 and 1550 Å) associated with this sunspot as well as the fine structure of the velocity field. The spiral fibril pattern observed in Hα is consistent with a constant α force-free field extrapolation of the photospheric magnetic field, as demonstrated by Schmieder et al. (1989). For the first time evidence is found that C IV fibrils near spots follow the field lines parallel to the chromospheric Hα fibrils. The observed large scale pattern of redshifts and blueshifts in the vicinity of the sunspot is stable and conforms to the typical Evershed flow pattern of radial outflow at the photospheric levels and radial inflows at the chromospheric and transition region levels. The three dimensional velocity vectors associated with this flow have been derived under the assumption of an axially symmetric Evershed flow. Radial outflows of up to 1.1 km s^{-1} are found in the photosphere, inflows of up to 2.6 km s^{-1} in the H$\alpha \pm 0.3$ Å chromosphere and inflows of up to 17 km s^{-1} in the C IV transition region. Upflows up to 11–17 km s^{-1} are observed above the umbra in C IV although these upflows are not associated with the Evershed flow. The Hα flow pattern follows the spiral pattern outlined by the fibrils but the C IV flow vectors may exhibit the opposite rotational sense. Evershed flow channels in Hα and C IV show temporal variations that may be attributed to a quasi-oscillatory behaviour. Supersonic downflows are found in the sunspot penumbra throughout the three day period analyzed.

Key words: the sun: sunspots – the sun: chromosphere – the sun: magnetic field – the sun: evershed flow

1. Introduction

Sunspots are one of the most highly organized phenomena observed on the sun. They are characterized by intense concentrations of magnetic field that have yet to receive a convincing physical explanation. Many spots are nearly circular and are often surrounded by a penumbra made up of radially elongated structures which also demonstrate a certain degree of axial symmetry. Observations at high spatial resolution demonstrate the existence of considerable fine scale detail in the large scale structure. There is also a large scale flow pattern, called the Evershed flow, that is associated with the sunspot and is almost certainly the result of the magnetic field organization.

At photospheric levels the flow pattern consists of a radial horizontal outflow from the sunspot to the surroundings, while at chromospheric levels, the direction is reversed and material flows into the sunspot umbra. Alissandrakis et al. (1988) have recently shown that at transition zone temperatures (10^5 K), the flow has the same characteristics as the inward chromospheric flow, with a higher flow velocity. When observed at high resolution, the flow pattern itself is more complex. For example, Haugen (1969) reports large variations in Hα velocities about the mean, including velocities in the opposite direction from the general chromospheric Evershed flow. Maltby (1975) demonstrated that the flow is concentrated into channels with typical widths of 1000 km. Sunspot spectra show the presence of asymmetries and multiple components, both in the photosphere (Bumba, 1960) and in the transition region (Brueckner, 1981; Dere, 1982; Nicolas et al., 1982; Kjeldseth Moe et al., 1988). Some of these effects can perhaps be explained by variations in the source function and the optical depth along the line of sight and by the existence of unresolved structures with different velocities. Nevertheless, the Evershed flow pattern provides a useful description of many aspects of the observed flow pattern. The syphon mechanism (Meyer and Schmidt, 1968; Alissandrakis et al., 1988) and convective roll motions (Danielson, 1961; Galloway, 1975) have been proposed to explain the cause of these flows. In this paper we examine the flow pattern around a sunspot at photospheric, chromospheric and transition zone temperatures in order to deduce the characteristics of the associated Evershed flow as well as deviations from this flow.

2. Observations and data reduction

The sunspot in active region NOAA 4682 was observed at ultraviolet wavelengths by the HRTS aboard the Space Shuttle Spacelab 2 mission and at visible wavelengths by coordinated ground based instruments at the Meudon Observatory. The

Send offprint requests to: B. Schmieder

Spacelab 2 version of the HRTS (Brueckner et al., 1986) includes a 30 cm Gregorian telescope, a tandem-Wadsworth UV spectrograph (Brueckner and Bartoe, 1983), a broadband UV spectroheliograph and an Hα viewing system. The spectrograph slit has an equivalent length of 920″ and width of 0″.5. This study is largely based on the analysis of the profiles of the C IV lines at 1548 Å and 1550 Å formed at 10^5 K in the transition zone. Narrow chromospheric lines of Si I in this wavelength region are used to derive a wavelength scale that is assumed to be nearly absolute because the Doppler shifts observed in this line are quite small, usually less than 1 km s^{-1}. Two dimensional arrays of line profiles were obtained by repeatedly stepping the slit in 2″ or 3″ increments. Data reduction procedures are described in detail by Dere et al. (1984). By taking the zero, first and second order wavelength moments of the C IV profiles, images of the integrated intensity, Doppler shift and line width are derived. In this paper, time series of profiles associated with flow patterns displayed in the images have also been analyzed in detail for the Rev 56 observations, including the high speed downflow profiles. Rastered spectra were obtained during three different Spacelab 2 orbits spanning three days. These data sets are referred to here by their "Rev" or orbit number (see Table 1).

Table 1. HRTS observations

Rev.	Date	UT	Spot coordinates	Heliocentric distance	Step size	Raster width
43	August 1	13:38–14:06	E 21 S 15	29	3″	30″
		14:16–14:20			2″	20″
56	August 2	09:17:28–09:18:15	E 11 S 15	23	3″	30″
		09:18:26–09:19:12				
		09:21:22–09:22:03				
		09:22:20–09:23:01				
		09:27:14–09:28:53				
		09:28:13–09:29:58				
		09:29:07–09:29:58	(1)			
		09:30:01–09:30:43	(1)			
67	August 3	02:14–02:38	E 01 S 15	21	2″	60″

(1) Unstable pointing

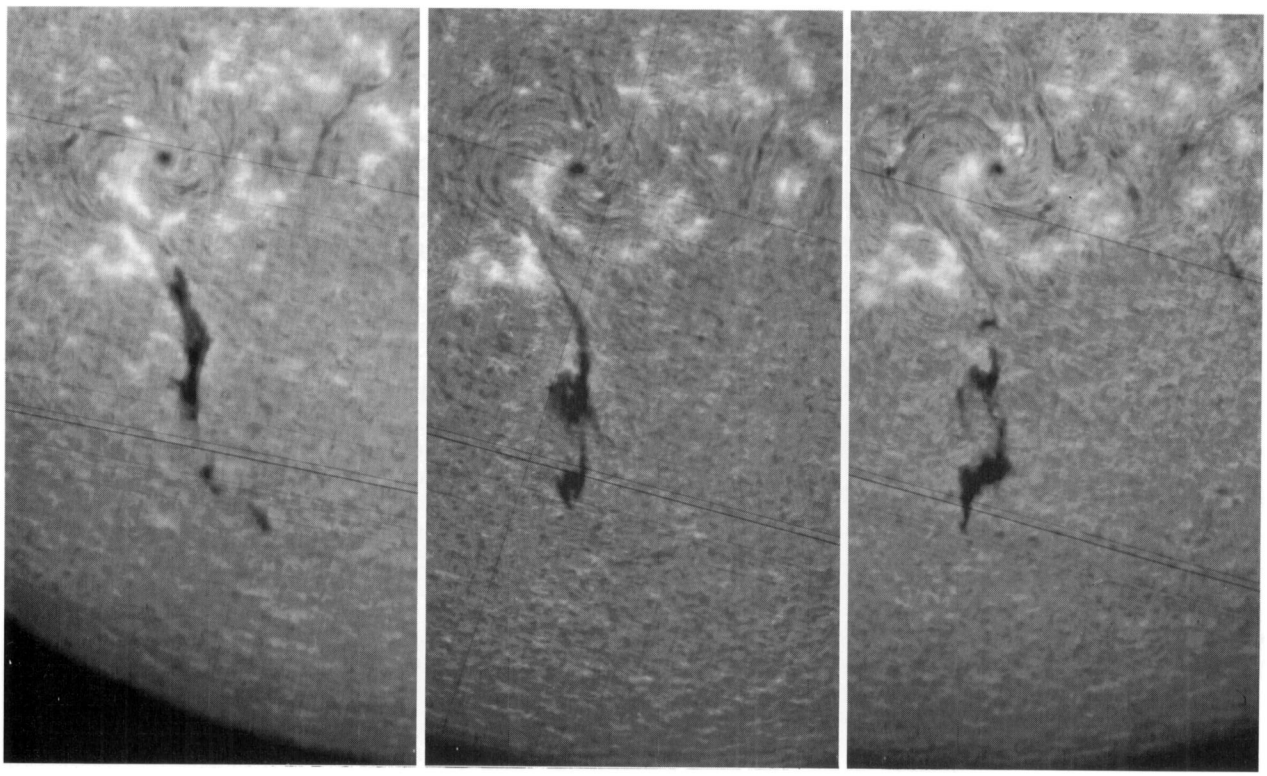

Fig. 1. Meudon spectroheliograms showing the stability of Active Region 4682 over the period August 1–3, 1985

Solar observations at the Meudon Observatory were obtained with the full-disk spectroheliograph, the photospheric magnetograph, and the Multichannel Subtractive Double Pass Spectrograph (MSDP). The spectroheliograph routinely records 1 to 5 Hα and Ca II K_3 spectrograms daily. Portions of the Hα spectrograms that include the active region are shown in Fig. 1. Three sets of observations were made with the Meudon magnetograph on August 2 at 9:42, 13:04, and 15:15 UT. Intensity and line-of-sight velocity maps as well as magnetograms in the photospheric line Fe I 6173 Å were obtained and analysed. The set at 9:42 UT is nearly simultaneous with the HRTS observations made during Rev 56.

The MSDP records a two dimensional $8' \times 1'$ field of the solar surface with good spatial ($\sim 2''$) and temporal (10 s) resolution. Observations of the same region are simultaneously obtained in 9 wavelengths in the Hα line, from which a two dimensional set of profiles are reconstructed. Maps of intensity fluctuations and Doppler shifts are derived using the standard method (Mein, 1977; Schmieder et al., 1989). By displacing the entrance slit, a large field of view ($(8' \times 5'$) covering the entire active region is obtained each 60 s. The region around the sunspot is covered with two $8' \times 1'$ elementary fields of view which were combined by two dimension cross-correlation techniques. During the period of interest, the MSDP spectrograph was operating on August 2 between 9:20 (Rev 56) and 15:14 UT (exact times are given in Fig. 7).

The MSDP and the HRTS images were coaligned by means of the known orientation of the images with respect to solar north and by the outline of the sunspot in the MSDP image in the continuum near Hα and in the ultraviolet HRTS image of Si I; the relative position of the images was also checked by comparing the plage in C IV and at the center of Hα. For the HRTS exposure times used for the Rev 56 data set, the Si I lines are not well exposed and consequently the outline of the sunspot is not especially well defined. We estimate that the coalignment in Rev 56 is accurate to about 3″, which is the HRTS raster step size for this data set. In Fig. 2, the Meudon MSDP Hα images and the HRTS images are displayed. The HRTS images presented in Fig. 2 have been rotated so that solar north is to the top in all the images.

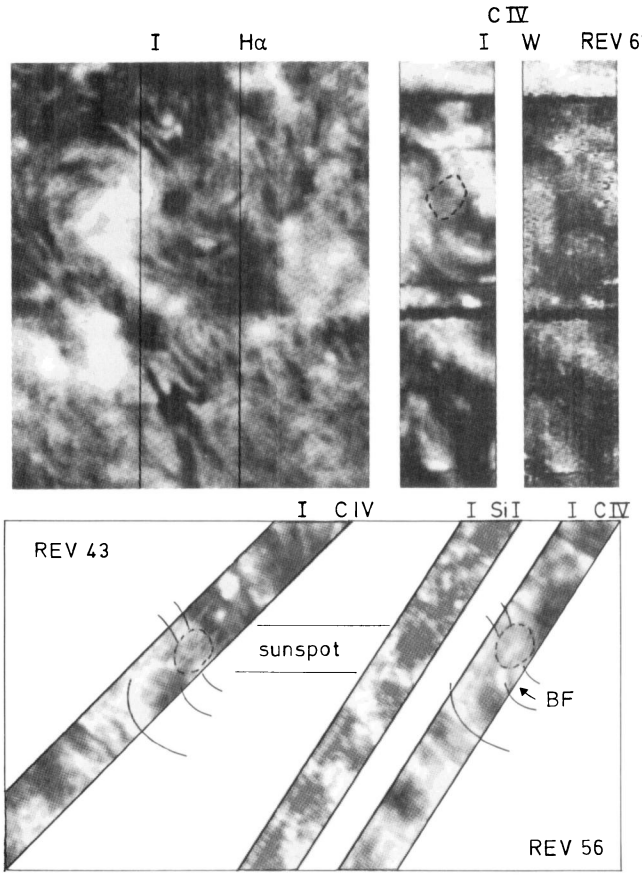

Fig. 2. The active Region 4682 observed with the MSDP instrument at Meudon in Hα and with the HRTS instrument aboard Spacelab 2 in C IV. The top row shows images of Hα line center intensity (August 2, 1985 at 09:54 UT) and C IV intensity and line width (Revolution 67, August 3 at 02:14 UT). The bottom row shows C IV intensity (Revolution 43, August 1 at 13:38 UT) as well as Si I intensity and C IV intensity (Revolution 56 on August 2 at 09:17 UT). The size of the Hα image is 225″ by 270″. The field of view of the HRTS August 3 image has been marked on the Hα image. All images are oriented with solar north up, solar west to the right

3. Spatial structure of the active region

The active region NOAA 4682 was observed during four consecutive rotations (1762–1765) with the Meudon spectroheliograph. The birth, development and final disappearance of the sunspot was followed, as well as the evolution of a filament situated in the active region (Schmieder et al., 1989, 1990). The Hα fibrils around the sunspot were initially radial, but subsequently formed a spiral structure at the same time as a plage filament appeared (rotation 1764, July 29 through August 6; see Fig. 1). At the end of the observating period (rotation 1765) the Hα topology changed dramatically, implying a complete restructuring of the magnetic field. The sunspot disappeared and the plage filament was replaced by a portion of an extended quiescent filament.

The Hα spectroheliograms show that the general pattern around the sunspot is remarkably stable during rotation 1764 which included the Spacelab 2 interval (Fig. 1). The longitudinal magnetic field polarity is negative in the sunspot and positive in the faculae south of the spot; the filament lies between the two. The spot is a leading spot with clockwise chromospheric vortex motion, and it is in a decreasing phase as suggested by the polarity rule (Martres et al., 1973). The C IV intensity map (Rev 67) clearly shows dark and bright fibrils around the spot that can be identified with the Hα fibrils (Fig. 2). On the other C IV maps (Rev 43 and Rev 56), such an identification is only suggested because the pattern can be seen only in a reduced field of view.

In a previous paper (Schmieder et al., 1989), the extrapolation of the magnetic field above the photosphere of Active Region 4682 was calculated for comparison with the observed structure of the filament extending to the south. The extrapolated fields were calculated under the force-free field assumption ($\nabla \times \mathbf{B} = \alpha \mathbf{B}$) using the Fourier transform method developed by Alissandrakis (1981). The spiral pattern of the Hα fibrils indicated that the fields at chromospheric levels were not potential ($\nabla \times \mathbf{B} \neq 0$). A single constant value of α was found that reproduced the shear observed in Hα over the complete field of view of the Hα map (Fig. 2). A representation of the extrapolated field at a height of 2000 km above the photosphere for $\alpha = (190\ \mathrm{Mm})^{-1}$ is displayed in Fig. 3. Computed field maps at greater heights are smoother but show the same basic behaviour.

While sunspots are some of the more pronounced features seen on the solar disk in photospheric and chromospheric emissions, they are particularly undistinguished in transition zone line intensities. The HRTS C IV rasters of the sunspot in AR 4682 do

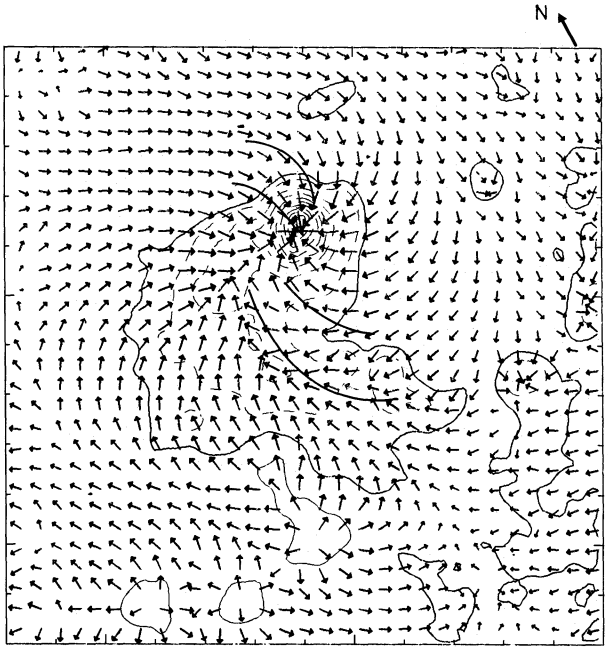

Fig. 3. A linear force free field magnetic field extrapolation of the photospheric magnetic field observed at Meudon at a height of 2000 km (from Schmieder et al., 1989). The arrows drawn every 8″ indicate the direction of the horizontal field, the dashed contours represent the isocontours of the vertical component. The heavy line indicates the position of the fibrils visible on the Revolution 67 intensity map

not show any characteristic intensity pattern that could be associated with the sunspot itself (Fig. 2). In Rev 43, there is a relatively low intensity pattern in the region of the sunspot. In Rev 56, there is a relatively bright feature near the center of the sunspot and in Rev 67 there is an extended patch of about average brightness that overlies the sunspot.

Athay et al. (1983) were unable to discern any typical intensity pattern associated with sunspots observed by SMM in C IV but did notice that a train of several bright knots often encompassed the spot just beyond the penumbra. At the south of the spot, a very bright C IV arch (BF in Fig. 2), characterized by broad line profiles (see the Doppler width map in Fig. 10) is associated with newly emerging magnetic flux. A spectacular example examined in detail by Brueckner et al. (1988) is to the northwest of the spot in Rev 67 (Fig. 2). This suggests that the bright knots surrounding sunspots seen by Athay et al. (1983) may be related to emerging magnetic flux.

The HRTS raster in Rev 67 is the widest (60″) of those used in this study. The intensity images in this orbit show elongated C IV fibrils that are parallel to the underlying Hα fibrils. Although Athay et al. (1983) have noted the existence of active region loops in C IV, this is apparently the first set of observations which shows the fibril structure evident in Hα around sunspots to extend to transition zone temperatures.

4. The velocity field around the sunspot

4.1. The large scale velocity pattern

Figure 4 shows velocity maps for C IV on August 1 to 3, together with photospheric and Hα ± 0.3 Å maps on August 2 and a sunspot drawing for the same date. The maps, except for the August 3 C IV map, are averages of several observations; this was done in order to enhance the steady features of the flow pattern and reduce the effect of oscillatory and transient phenomena as well as noise and bad data. The C IV velocity contours were drawn under the assumption of zero average velocity over the entire HRTS field of view in order to have the same frame of reference as in our previous study of the C IV Evershed flow (Alissandrakis et al., 1988). The center of the spot was determined as the center of gravity of the intensity map in the continuum near Hα.

The main features of the large scale flow pattern observed at photospheric, chromospheric and transition zone temperatures are consistent with a radially symmetric flow of plasma into and out of the sunspot. In the photosphere, a crescent shaped region of blueshift in areas on the side of the sunspot toward the disk center and a region of redshift on the opposite side are observed. These are consistent with the usual outward motion in the photospheric Evershed flow pattern. The pattern is nearly antisymmetric with respect to the spot center, an indication that the vertical component of the flow velocity is very small (Dialetis et al., 1985).

The Evershed pattern in Hα is also quite clear; however, here the vertical velocity component is not negligible and thus the most prominent feature is the large area of redshifted emission on the diskward side of the sunspot, while the blueshifted region on the limbward side is much less prominent. The redshifted region shows considerable structure with 4 peaks ("a"–"d" in Fig. 4), which indicates a departure from strict axial symmetry (the peak at the upper left of the figure is not associated with the Evershed flow as will be discussed below). The size of the velocity pattern is clearly larger in Hα than in the photosphere, with the velocity peaks further away from the spot center. The redshifted peak is located just outside the edge of the photospheric penumbra.

The observed signature of the Evershed flow in C IV consists of a region of strong redshift on the diskward side of the spot and a much weaker blueshift region on the limbward side. The spatial extent of the pattern is at least as large as that of the chromosphere. Some structures in the redshifted region on August 2 ("C" and "F" in Fig. 4) are nearly cospatial with the Hα structures ("b" and "c" respectively) but other portions of the pattern show no close correlation with Hα (e.g. the C IV structure "E"). In agreement with the observations of Mein et al. (1982) and Alissandrakis et al. (1988), positive velocities (upflows) are observed above the spot in all three C IV maps. The peak velocity is about 13 km s^{-1}, relative to Si I), which is consistent with the values of Alissandrakis et al. (1988). The position of the peak velocity changes from one day to the next and it shows a tendency to avoid the center of the umbra. As pointed out by Alissandrakis et al. (1988), this upflow is not part of the classic Evershed effect.

With regard to the strong subsonic component of the C IV profiles, there does not appear to be a pattern characteristic of sunspots in general. The sunspots in the first (Nicolas et al., 1982; Dere, 1982) and second (Brueckner, 1981) HRTS rocket flights show redshifts of 0–30 km s^{-1}, while an Evershed type inflow has been reported by Nicolas and Kjeldseth-Moe (1981) and Athay et al. (1982). Gurman and Athay (1983) found that the C IV velocities in 8 sunspots observed by SMM were, on the average, equal to those in the quiet sun which show a redshift of about 5 km s^{-1}. On the other hand, Mein et al. (1982) and Alissandrakis et al. (1988) both find blueshifts of 10–33 km s^{-1} (relative to the average velocity over the whole field) associated with several sunspots. Gurman et al. (1982) have detected sunspot oscillations in transition region lines with an average peak-to-peak amplitude of 4 km s^{-1} and a period of about 150 s. It is possible that a clearer

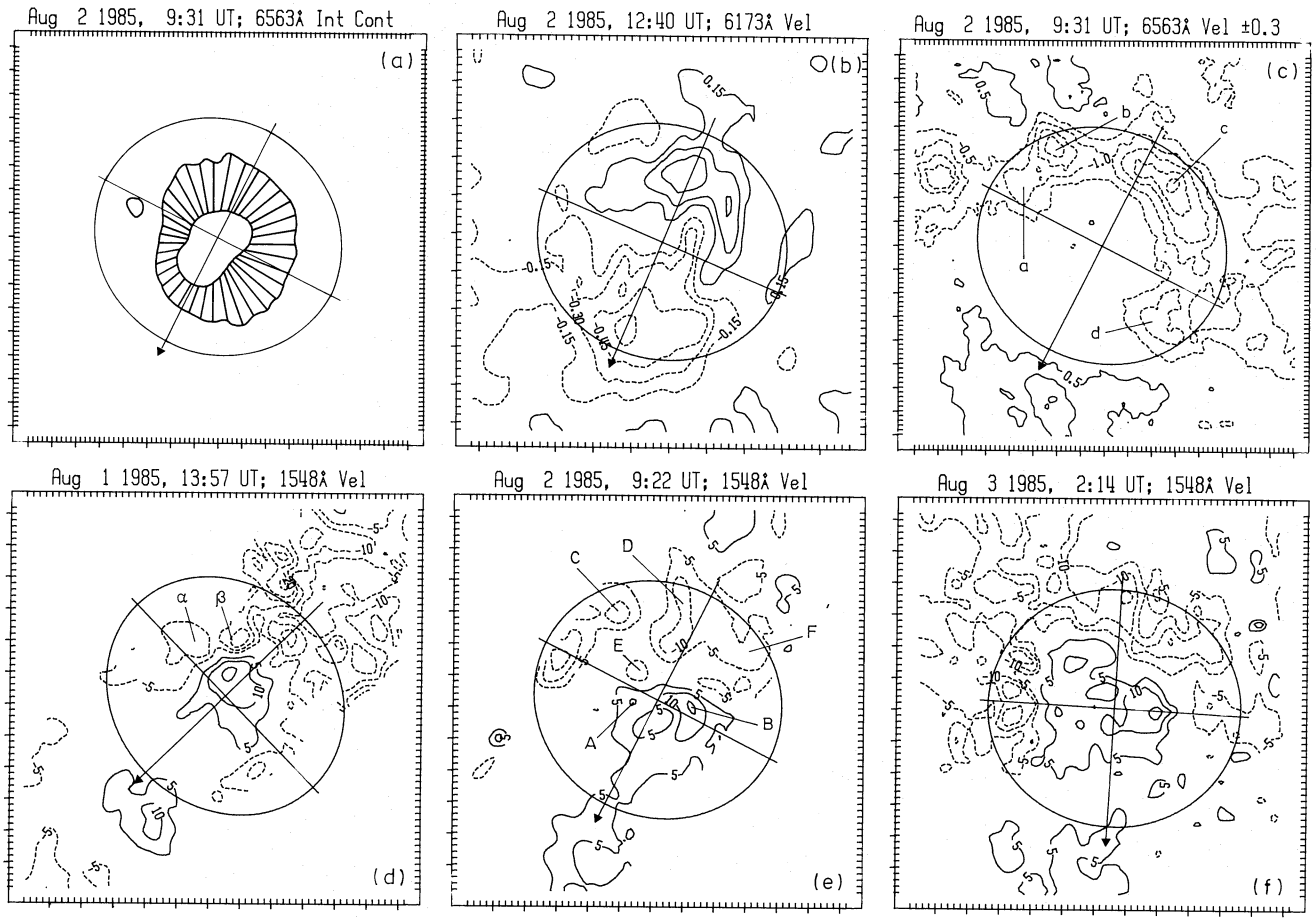

Fig. 4a–f. Line of sight velocity maps in the photosphere (average of three observations), the chromosphere (average of seven observations) and transition region (average of two observations for August 1, six observations on August 2, a single observation on August 3). A drawing of the sunspot from observations in the continuum near Hα is also shown. The ellipse is the projection on the plane of the sky of a 20″ radius circle, centered on the assumed spot center. High speed downflows were detected in regions α and β (August 1), in region E (August 2) and in the region just inside the western part of the circle on the August 3 map. All maps are oriented with solar north up and west right, while the direction of the limb is shown by the arrows. Dashed contours are redshifts. The image size is 60″ × 60″

picture of the steady-state subsonic sunspot flow pattern would emerge if the oscillatory component were removed from the various sunspot data sets.

4.2. *Velocity vectors in the* Fe I *photosphere, Hα chromosphere, and the* C IV *transition zone*

Dialetis et al. (1985) have developed a technique for reconstructing the velocity vector of the Evershed flow under the assumption that the velocity field is axially symmetric and stable during the period in which the data were obtained. The formulation was applied to the sunspot flow patterns analyzed by Dialetis et al. (1985) and by Alissandrakis et al. (1988) and is now applied to the present data set. The radial, vertical and azimuthal components of the velocity are calculated by integrals of the observed two dimensional line-of-sight velocity components. In this coordinate system, positive radial velocities are inward toward the sunspot, positive vertical velocities are up from the solar surface and positive azimuthal velocities are clockwise. Errors in the derived velocities occur when the solar conditions do not conform to the assumptions of the model, i.e., a static, radially symmetric flow about the local vertical. For example, a statistical analysis by Bumba (1960) indicates that the axis of the flow could be inclined by as much as 30° from the vertical. In addition, the model does not reliably calculate the velocity components close to the center of the spot where the derived velocities are based only on a few data points. Figure 5 shows the residual velocities after the application of the model, together with the original line of sight velocity data for the three regions of the solar atmosphere. It is clear that the model accounts very well for the large scale components of the motion, while it does not adequately represent small scale components which are most conspicuous in Hα and C IV. The small features are not used for the computation of the velocity components, because our algorithm ignores all data that deviate from the assumption of axial symmetry by more than three standard deviations (c.f. Sect. 4 in Alissandrakis et al., 1988).

The rms of the residuals is 0.10 km s^{-1} for the photospheric data, 0.5 km s^{-1} for the chromospheric and 4 km s^{-1} for the transition region data. This increase reflects the increase of the line of sight velocity in the three layers and not a deterioration of the quality of the data. Error margins were computed as the changes in the deduced components of the velocity required to increase the rms value of the residuals by a factor of 2; these represent statistical deviations from the assumed azimuthal symmetry. Alternatively, error estimates can be obtained from the standard deviations of the components averaged over individual maps; these reflect time variations. The two estimates are very similar and their average is given below.

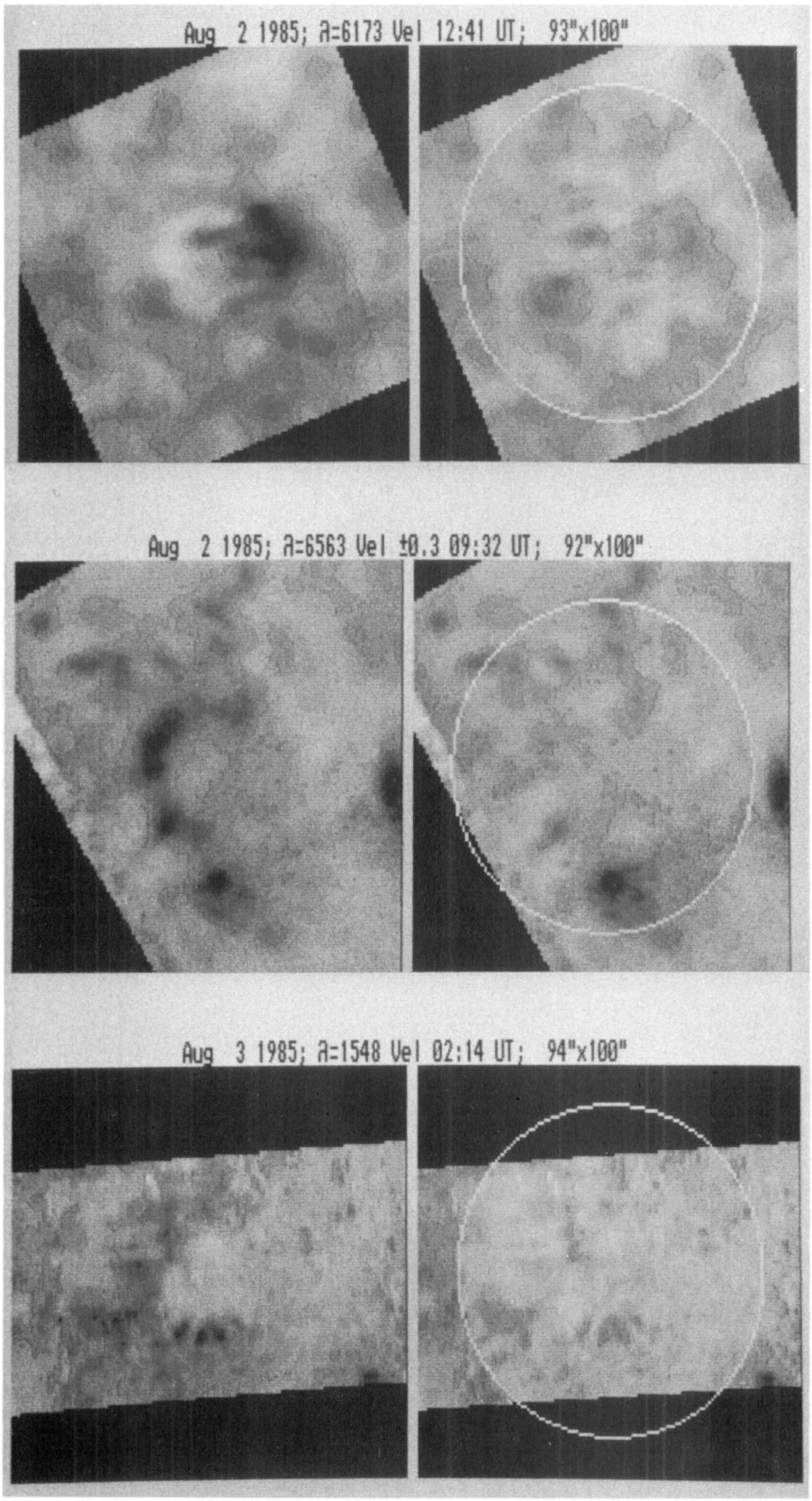

Fig. 5. Line of sight velocity maps before (left panels) and after (right panels, same intensity scale) the subtraction of the velocity vector computed with the procedure of Dialetis et al. (1985), for the photosphere, the chromosphere and the corona. The velocity vector was computed inside a circle of 40″ radius (white ellipse in the figure). The images are oriented with the solar limb to the right. Dark black regions represent missing data

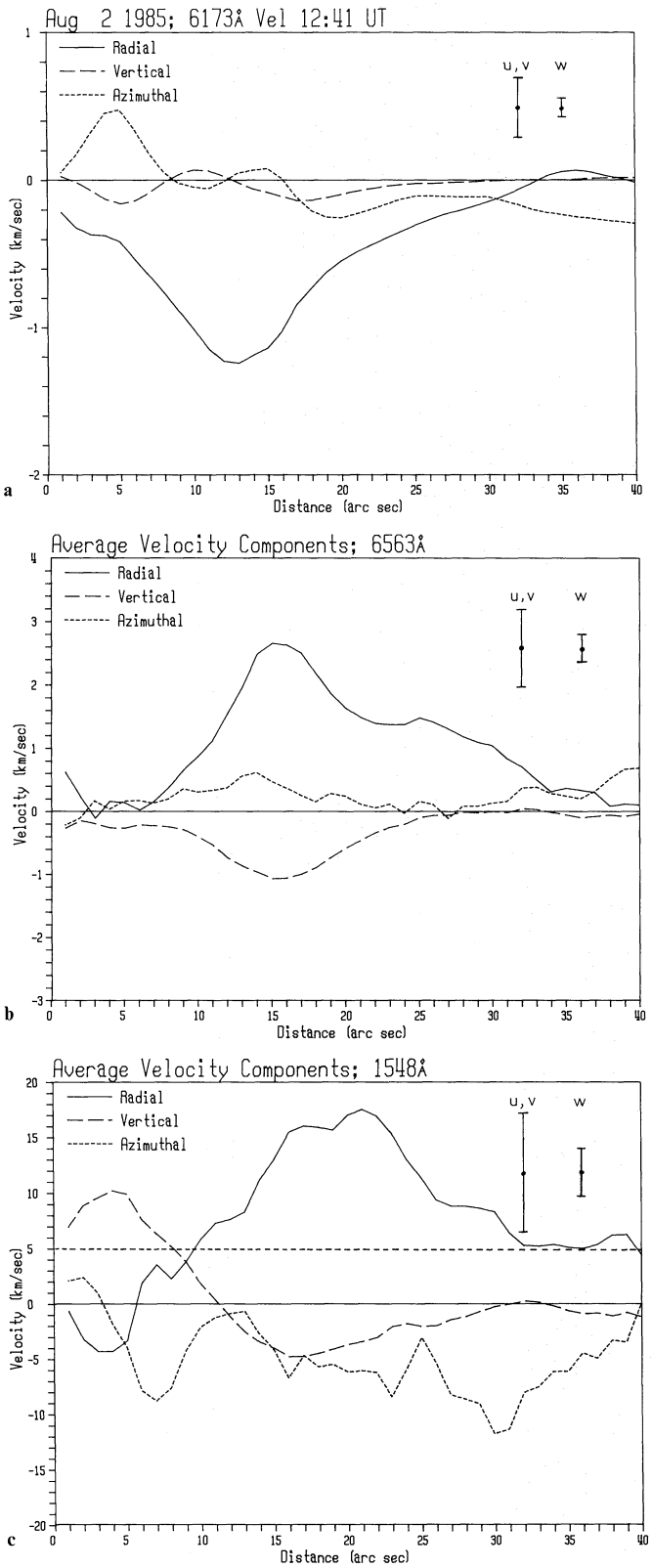

Fig. 6a–c. Components of the velocity vector as a function of distance from the center of the spot (Radial (u): solid line, azimuthal (v): dot-dashed line, vertical (w): dashed line). Positive radial component corresponds to inflow, positive vertical component to upflow and positive azimuthal component to clockwise motion. **a** Photosphere (Fe I 6173 Å) **b** Chromosphere (H$\alpha \pm 0.3$ Å) **c** Transition zone (C IV 1548, 1550 Å). The results shown are averages of computations from all available data. The dashed line shows the zero level of the vertical component in C IV relative to the Si I lines

Plots of the radial, vertical and azimuthal components of the photospheric Evershed flow velocities derived using Dialetis' technique from the average of the three Fe I 6173 Å observations on August 2, are shown in Fig. 6a. The estimated errors are 0.2 km s^{-1} for the radial and azimuthal components and 0.06 km s^{-1} for the vertical component. The velocity field is dominated by the radial outflow which peaks at a velocity of about 1.1 km s^{-1} about 12″ from the center of the spot and it is detectable out to about 30″ from spot center. Beyond 8″ the flow is radially outward and rising until about 12″ when the vertical velocity vector becomes negative and the flow becomes radially outward and downward, out to about 30″.

The H$\alpha \pm 0.3$ Å velocities on August 2 at 09:32 UT (average of seven maps obtained at about the same time as Rev 56), 12:21 UT and 15:15 UT have been used to calculate the velocity components for these individual times and for an average of the three observations. The average velocity components are shown in Fig. 6b. The estimated arrors are 0.6 km s^{-1} for the radial and azimuthal components and 0.2 km s^{-1}, for the vertical. Again, the radial component dominates and it is an inflow. It shows a maximum velocity of about 2.6 km s^{-1}, 15″ away from the spot center and extends to about 40″. The vertical component is predominantly negative, indicating a downward flow at distances up to 26″ from the spot center. Beyond that the flow is nearly horizontal. The peak of the vertical component is -1.1 km s^{-1} and occurs at a distance of 15″ from the center. The velocity is lower at H$\alpha \pm 0.6$ Å, consistent with previous measurements.

The transition region velocity components have been calculated from the observed C IV 1548 and 1550 Å line profiles during Revs 43 (two maps), 56 (six maps), and 67. The average velocities from the three data sets are shown in Fig. 6c; the data from Revs 43 and 56 do not cover the entire field of view and have therefore been given a lower weight in the averaging. The estimated errors are 5 km s^{-1}, for the radial and azimuthal component and 2 km s^{-1} for the vertical. The figure shows a strong inward radial component (the same sense as Hα) that extends beyond 40″ with velocities as high as 17 km s^{-1}, at a distance of about 20″ from the center. The vertical flow is positive (upward) near the center, due to the presence of blueshifted profiles there (cf. Fig. 4); outside the penumbra it is negative (downward) with a peak velocity of about -5 km s^{-1}. Our assumption that the average line of sight velocity is zero affects the computation of the vertical component only; if this assumption is dropped, a value of 5 km s^{-1} should be subtracted from this component and the velocity zero would be at the position shown by the dashed line in Fig. 6c.

The Evershed flow vectors should provide a map of the magnetic field vectors at the three atmospheric levels. In particular, the spiral pattern seen in Hα should be evident in the radial and azimuthal flow vectors. In all three layers the azimuthal component is small or comparable to the error margin. However, in the Hα data the flow vectors indicate a systematically positive (clockwise) spiral, while in the C IV data they indicate a systematically negative spiral. For a more reliable estimate of the field curvature we computed the angle between the horizontal velocity and the radial direction, averaged over the region around the radial velocity peak, where the Evershed signal is strongest. We obtained values of 1.4 ± 9, 8.2 ± 4, and -19 ± 4 degrees for the photosphere, chromosphere and transition region respectively. In the line of sight velocity maps the presence of an azimuthal component and its direction are reflected as an asymmetry with respect to an axis through the spot center and perpendicular to the limb (axis with the arrow in Fig. 4). An examination of the Hα map in Fig. 4 reveals

that the average velocity is indeed smaller (more negative) at the right of this axis, while the opposite is true for the C IV maps; this is consistent with the computed sign of the azimuthal component. The effect is visible on the other C IV maps we cannot exclude the possibility that small high-velocity structures but such as those in the August 3 map just inside the ellipse at the left, might influence this result; our algorithm tends to ignore such regions.

These results seem to indicate that the direction of the chromospheric flow is consistent with the spiral pattern of the chromospheric fibrils and the direction of the magnetic field in the chromosphere, which is twisted in the same sense (Fig. 3) and forms an angle of about 13 ± 5 degrees with the radial direction; a measurement of the azimuth of the transverse component of the field observed at Marshall SFC (courtesy of M. Hagyard) gives a value of 14 ± 2 degrees. However, it appears that the sense of twisting of the velocity field is reversed in the transition region. This is in apparent contradiction with the sense of twisting of the C IV fibrils (Sect. 3); however the fibrils are located much farther from the spot than the Evershed region. If this is indeed the case, it implies a shear of the magnetic field along the vertical direction.

The large scale properties of the Evershed flow deduced in the course of this study are remarkably similar to those of Alissandrakis et al. (1988) for the same atmospheric layers and of Dialetis et al. (1985) for the photosphere and the chromosphere. All three studies give similar values for the maximum radial velocity, they show a clear increase of the maximum velocity from the photosphere to the transition region and a similar increase of the distance of the maximum velocity from the spot center. The velocities are subsonic, with Mach numbers of about 0.15, 0.25, and 0.45 for the photosphere, the chromosphere and the transition region respectively (assuming sound velocity of 7, 11, and 37 km s^{-1}).

4.3. *Small scale structures in the velocity field*

The average Hα velocity map in Fig. 4 does not show the fine structure of the flow channels, which can be as narrow as 1″ (Maltby, 1975). Such channels are visible in Fig. 7, which includes all individual maps used in the present study. The best image in the series (at 12:20 UT) shows that the redshifted portion of the Evershed pattern consists of several small structures, superimposed on a diffuse background. The fine structures are elongated and their orientation with respect to the spot is roughly radial; their width is as small as 2″ and they are as long as 11″.

Changes in the flow structure over time are also evident. In agreement with Maltby (1975) who gave an upper limit of 2 h for the lifetime of the small scale flow structures, it can be seen that later in the day, at 12:20 UT and at 15:14 UT, entirely different structures appear in the velocity maps, than were present earlier at 9:20 UT. Changes also occur in these structures on shorter time scales. Apart from umbral oscillations that are clearly visible near the center of the velocity images of Fig. 7, the flow channels themselves show a quasi-oscillatory nature. Note, for example, the structure "a", which is prominent at 09:20 and 09:27 UT, barely visible at 09:26 UT and practically invisible in the other images. Structure "b" is quite prominent at 09:20, 09:26, 09:27, 09:29, and 09:54 UT and much less prominent at 09:28 and 09:30 UT, whereas the extended, arch-like structure "c" is very weak at 09:20

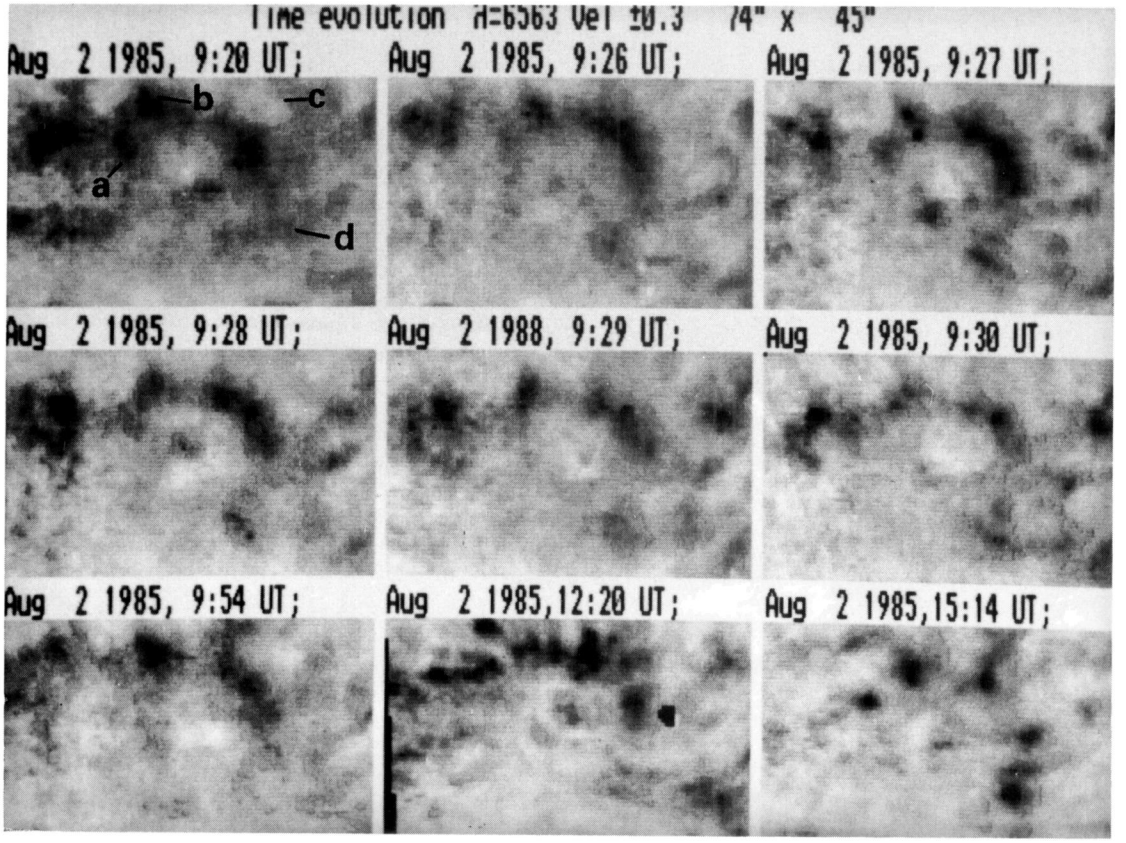

Fig. 7. Time evolution of the line of sight velocity in H$\alpha \pm 0.3$ Å. The spot is at the center of each panel. Dark black regions represend bad or missing data. Points 'a', 'b', 'c', 'd' (same as in Fig. 4) are regions of downflow (dark)

and 09:30 UT and very intense in the other images up to 09:54 UT. Other structures, such as "d", show a fairly smooth rise and decay in the interval from 09:20 to 09:54 UT. Although the time series is neither dense nor long enough to establish oscillation periods, periodicities of the order of 2 min may be seen. The oscillating elements are not in phase. Nor do the quasi-oscillations exhibit a wave-like character unless the wavelength is comparable to their radial extent, since the flow velocity in the entire structure rises and fades simultaneously. Thus they are probably not associated with penumbral waves.

The present HRTS C IV velocity data also show considerable spatial deviations from the idealized Evershed flow pattern, much more than the UVSP data used by Alissandrakis et al. (1988). In the velocity data used in this paper the fine structures are best visible in the map of Rev 67 (Figs. 4 and 5). The finest structures are those in the east, just inside the ellipse in Fig. 4. Their size is about 3″ by 6″ and their orientation radial. Kjeldseth-Moe et al. (1988) observed supersonic downflows in this region. These structures lie just outside the spot penumbra, in a region where small pores appeared and disappeared daily [see Fig. 1 of Kjeldseth-Moe et al. (1988) for a series of daily photospheric photographs]. Consequently, it is not clear that these fine structures are part of the Evershed flow. Also, due to the position of these structures with respect to the spot center and the direction of the limb, the radial component of the velocity is perpendicular to the line of sight; therefore what the observations show is a combination of the vertical and azimuthal components only. Fine structures are also visible in the region of the Evershed pattern, at the diskward side of the spot. These structures show no prominent elongation in the radial direction.

4.4. *Supersonic transition region downflows*

The characteristics of the velocity field near sunspots in the photosphere and the chromosphere are fairly well established. The situation is less clear in the transition region. HRTS observations of several sunspots indicate that they do have a distinctive signature in their transition region line profiles which show both an intense subsonic component and one or more weaker supersonic components. These observations include two separate sunspots observed during two rocket flights and the sunspot in AR 4682 seen in the extended series of Spacelab 2 spectra. The first rocket flight revealed several small regions of 100–150 km s^{-1} downflows over the umbra (Nicolas et al., 1982; Dere, 1982) while the second flight found downflows up to 175 km s^{-1} extending over a large complex sunspot containing a light bridge (Brueckner, 1981). The various spectra obtained during Spacelab 2 indicate that the sunspot in AR 4682 is essentially always associated with high speed downflows. The spatial distribution of these downflows is variable from orbit to orbit. Small regions of high speed downflow are seen in Revs 43 and 56 over the penumbra of the spot. Kjeldseth-Moe et al. (1988) have mapped the flows during Rev 67 and showed that the high speed downflows occur in a sheet-like structure on the edge of the sunspot umbra. In Rev 82 (August 4, 0100 UT), the high speed flows are spread out over the spot in a pattern similar to that found in the second rocket flight.

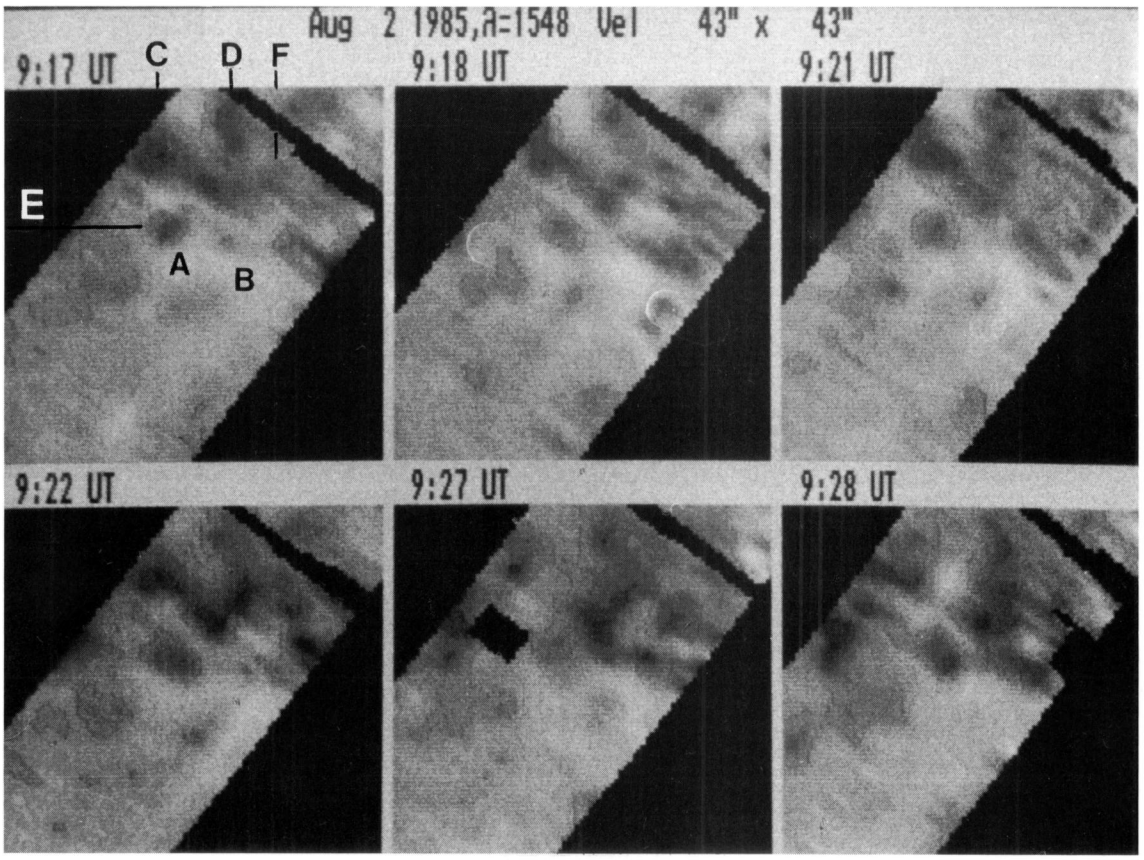

Fig. 8. Evolution with time of the C IV velocity pattern during Rev 56. Dark black regions represent bad or missing data. Regions 'A' and 'B' are upflows (light) and 'C', 'D', 'E', 'F' are downflows (dark)

These flows are observed over a large range of temperatures ($3\ 10^4$–$3\ 10^5$ K) with the largest velocities detected near 10^5 K (Kjeldseth-Moe et al., 1988).

4.5. C IV *line profiles and their temporal evolution during Revolution 56*

Figure 8 shows six frames of C IV velocity images obtained during Rev 56. Upflow regions ("A" and "B") and the regions of Evershed redshift ("C" and "D") show scales of 5″ while the high speed downflow region ("E", see next section) has a scale of 2.5″. Plots of line of sight velocity versus time for these regions are shown in Fig. 9. We should also mention that region "C" is cospatial with the Hα region "b" and region "F" very close to the Hα region "c", as we noted already in Sect. 4.1.

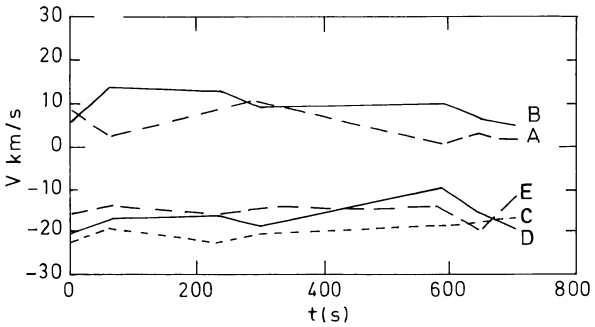

Fig. 9. Plots of line of sight velocity as a function of time for five C IV features observed during Rev 56

The observed transition zone flow field has been determined through the calculation of the first order moment of the C IV profiles. For near-Gaussian profiles this procedure gives satisfactory results, however it can mask multiple velocity components along the line-of-sight. Therefore, it is worthwhile to examine the profiles in detail since multiple components are commonly seen in sunspot spectra and in profiles whose velocity moment indicates a net blueshift. At the same time, since several rasters of the Spot region were obtained in the course of Rev 56 (Table 1), it is also interesting to study the temporal evolution of the profiles, especially in the light of possible sunspot oscillations which could distort the velocity measurements in the sunspot.

In Fig. 10 we display C IV profiles obtained in a 3″ step raster across the sunspot in Rev 56 at 9:18 UT on August 2. Each exposure was 5 s long. To the right are images of the intensity, velocity and line-width moments. We have selected 5 regions, labelled "A" through "E", in Figs. 8 and 10 for a more detailed examination. Figure 11 shows the evolution of the profiles at these 5 points. It should be noted that pointing stability was maintained to better than 2″ during the first 4 exposures but then gradually deteriorated through the remainder of the orbit.

Regions "A" and "B" are sites of blueshifts in the sunspot umbra. Both regions appear to have weak red- or unshifted components in addition to the stronger blueshifted components. A net blue shift is maintained throughout the observing period. If there is an oscillatory component, which is not clear, it would appear to be out of phase at points "A" and "B".

Regions "C" and "D" are sites of strong penumbral redshifts associated with the Evershed flow and directly over regions of strong Evershed redshifts in Hα. The profiles shown in Fig. 11, which reflect the generally noisy character of this data set, do not

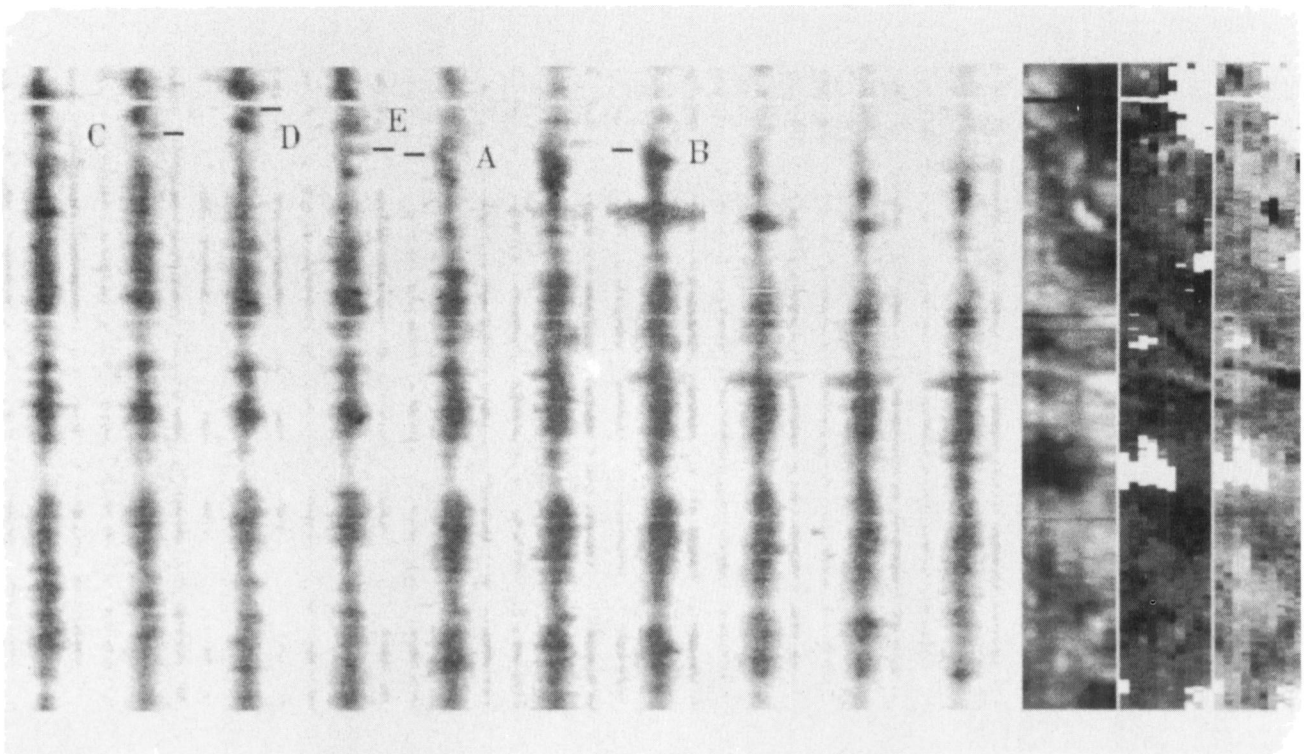

Fig. 10. C IV spectra through the sunspot observed on August 2, 9:17:41 UT during Rev 56 (left panels). Intensity, velocity and line-width maps in C IV and intensity map in Si I are shown in the right panels. The shape of the sunspot is well defined in the Si I intensity map. A, B and E are points in the umbea and C and D are in the penumbra of the sunspot. Notice the large broadening of the line in the seventh spectrum below B, corresponding to the brighter feature BF in Fig. 2

show any strong evidence for multiple components. The redshifts are fairly strong and are seen throughout the observing period.

Region "E" is located over the penumbra and contains the only supersonic downflows observed near this sunspot during Rev 56. The profile show significant intensity in the 30–70 km s^{-1} range, but there is no visible emission beyond 100 km s^{-1}. This strong downflow is present throughout the observing period.

5. Discussion

We have not attempted to derive the flow velocities along individual flux tubes and doubt that the data is sufficient to support such an effort. The radial component of the velocity vector varies with distance and temperature in a manner consistent with the predictions of models based on the assumption of subsonic siphon flow along the lines of force of the magnetic field (Alissandrakis et al., 1988). The velocities in C IV are almost an order of magnitude greater than in Hα. Similar ratios between C IV and Hα velocities have been observed in filaments (Schmieder et al., 1984) and in facular regions (Malherbe et al., 1987). Typical densities in chromospheric and active region structures indicate that the mass flux at these two temperatures are comparable but it is not clear that this would support a model where the chromospheric flow is heated to become the transition region flow. Rather, the Hα and C IV images indicate that the flows are along nearly isothermal flux tubes, with the strongest temperature

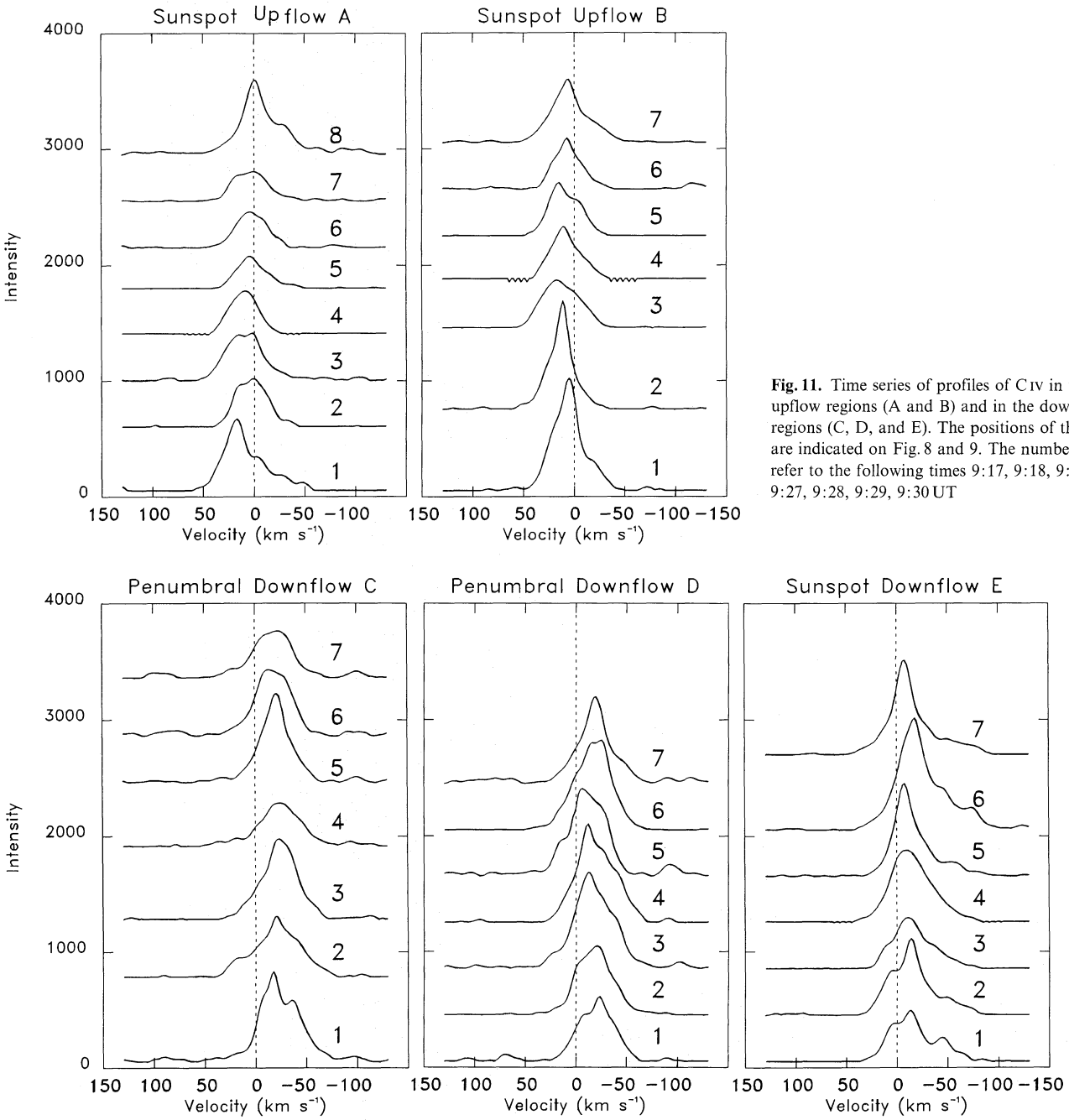

Fig. 11. Time series of profiles of C IV in the upflow regions (A and B) and in the downflow regions (C, D, and E). The positions of the regions are indicated on Fig. 8 and 9. The numbers 1–8 refer to the following times 9:17, 9:18, 9:21, 9:22, 9:27, 9:28, 9:29, 9:30 UT

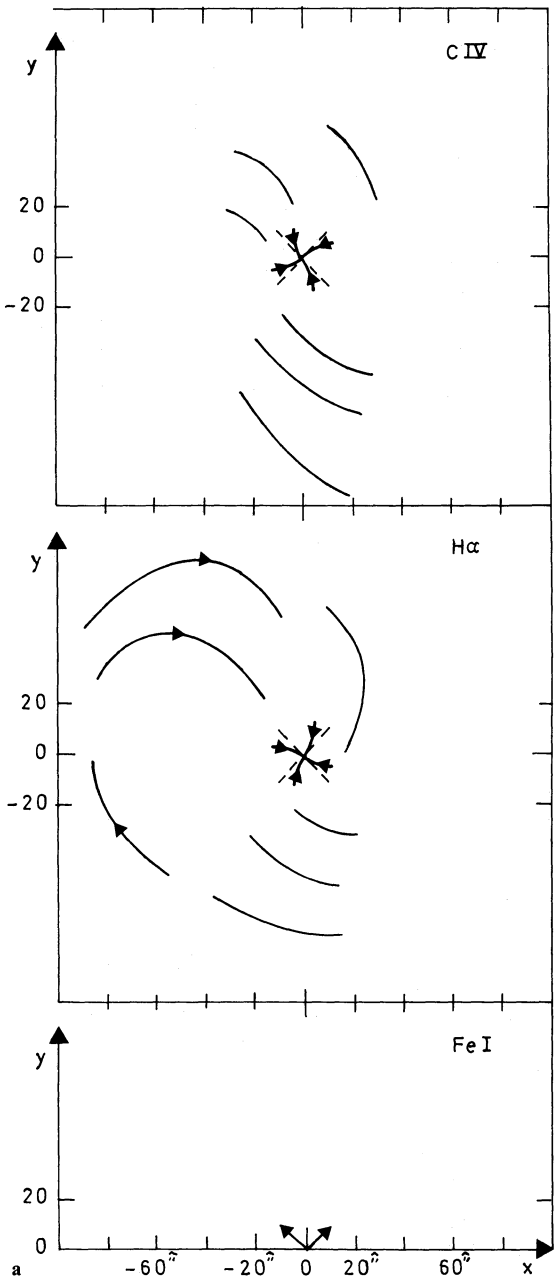

Fig. 12a and b. Sketches in plane x, y (**a**) and in plane x, z (**b**) of the observed flows at three levels of the atmosphere (Fe I photosphere, Hα chromosphere, C IV transition region). The orientation of the fibrils of the active region is also shown in (**a**)

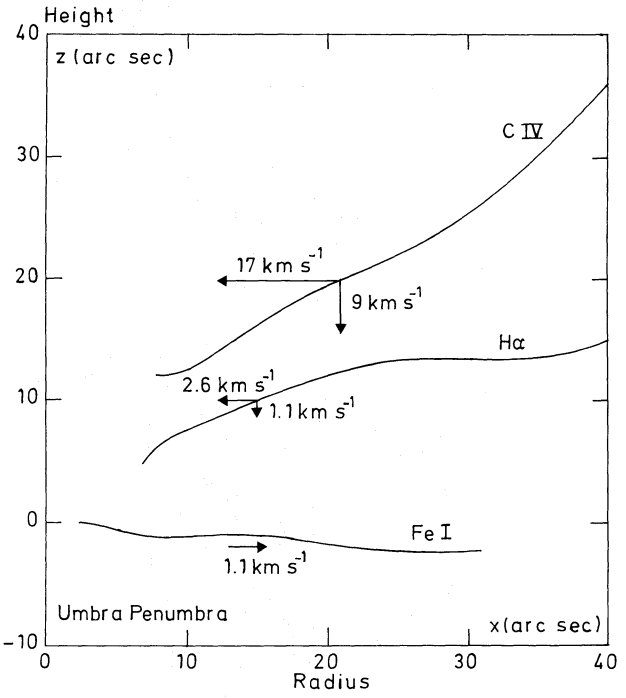

Fig. 12b

gradients perpendicular to the magnetic field. Hot and cold threads could exist close to each other because of the poor efficiency of the transverse heat conduction (Démoulin et al., 1987), although it is not clear what could cause the variation in physical conditions in neighboring flux tubes.

By integrating the radial and vertical velocities, it is possible to determine the shape of the streamlines in a vertical plane. A sketch of the observed flows is presented in Fig. 12. The heights of the individual field lines are relative and have been chosen to produce a reasonable interpretation of the field curvature. They indicate that the source of the C IV flows is located at a considerable distance from the sunspot.

Our detailed examination of C IV line profiles in the sunspot region during Rev 56 showed only one region where the profile had a component of supersonic downflow. This region was located over the spot penumbra and had no apparent association with the Evershed flow. Supersonic downflows were more abundant in the same spot during Rev's 43 and 67 (Kjeldseth-Moe et al., 1988; see also Fig. 4), which indicates the transient nature of these phenomena. It is interesting to know that these downflows were located in the region of the Evershed flow. The supersonic flows in Rev 56 and especially in Rev 43 occur in an area where the line-of-sight is nearly perpendicular to the direction of the magnetic field. If the flows are following the large scale magnetic field then ther velocity is considerably higher than the values quoted. Otherwise, it is possible that they follow small scale flux tubes that do not conform to the large scale field pattern.

Acknowledgements. The authors wish to thank Dr. J. Rayrole from Meudon and Dr. M. Hagyard from Marshall for providing magnetic data and Dr. M. Raadu for fruitful discussions. Travel funds for this research have been provided in part through the bilateral scientific exchange program between France and Greece.

References

Alissandrakis, C.E.: 1981, *Astron. Astrophys.* **100**, 197
Alissandrakis, C.E., Dialetis, D., Mein, P., Schmieder, B., Simon, G.: 1988, *Astron. Astrophys.* **201**, 339
Athay, R.G., Gurman, J.B., Henze, W., Shine, R.A.: 1983, *Astrophys. J.* **269**, 706
Brueckner, G.E.: 1981, in *Solar Active Regions*, ed. F.Q. Orrall, Colorado Associated University Press, Boulder
Brueckner, G.E., Bartoe, J.-D.F.: 1983, *Astrophys. J.* **272**, 947
Brueckner, G.E., Bartoe, J.-D.F., Cook, J.W., Dere, K.P., Socker, D.G.: 1986, *Adv. Space Res.* **6**, 263

Brueckner, G.E., Bartoe, J.-D.F., Cook, J.W., Dere, K.P., Socker, D.G., Kurokawa, H., McCabe, M.: 1988, *Astrophys. J.* **335**, 986
Bumba, V.: 1960, *Izv. Kryms. Astrofiz. Observ.* **23**, 212, 253, 277; see also Schröter, E.H.: 1967, in *Solar Physics*, ed. J.N. Xanthakis, Interscience, New York, p. 325
Danielson, R.E.: 1961, *Astrophys. J.* **134**, 289
Démoulin, P., Raadu, M.A., Malherbe, J.M., Schmieder, B.: 1987, *Astron. Astrophys.* **183**, 142
Dere, K.P.: 1982, *Solar Phys.* **77**, 77
Dere, K.P., Bartoe, J.-D.F., Brueckner, G.E.: 1984, *Astrophys. J.* **281**, 870
Dialetis, D., Mein, P., Alissandrakis, C.E.: 1985, *Astron. Astrophys.* **147**, 92
Galloway, D.J.: 1975, *Solar Phys.* **44**, 409
Gurman, J.B., Athay, R.G.: 1983, *Astrophys. J.* **273**, 374
Gurman, J.B., Leibacher, J.W., Shine, R.A., Woodgate, B.E., Henze, W.: 1982, *Astrophys. J.* **253**, 939
Haugen, E.: 1969, *Solar Phys.* **9**, 88
Kjeldseth-Moe, O., Brynildsen, N.F., Brekke, P., Engvold, O., Maltby, P., Bartoe, J.-D.F., Brueckner, G.E., Cook, J.W., Dere, K.P., Socker, D.G.: 1988, *Astrophys. J.* **334**, 1066
Malherbe, J.M., Schmieder, B., Simon, G., Mein, P., Tandberg-Hansen, E.: 1987, *Solar Phys.* **112**, 233
Maltby, P.: 1975, *Solar Phys.* **43**, 91
Martres, M.J., Soru-Escaut, I., Rayrole, J.: 1973, *Solar Phys.* **32**, 363
Mein, P.: 1977, *Solar Phys.* **54**, 45
Mein, P., Simon, G., Vial, J.C., Shine, R.A.: 1982, *Astron. Astrophys.* **111**, 136
Meyer, F., Schmidt, H.U.: 1968, *Z. Angew. Math. Mech.* **48**, 218
Nicolas, K.R., Kjeldseth-Moe, O.: 1981, in *The Physics of Sunspots*, eds. L.E. Cram, J.H. Thomas, Sacramento Peak Observatory, Sunspot
Nicolas, K.R., Kjeldseth-Moe, O., Bartoe, J.-D.F., Brueckner, G.E.: 1982, *Solar Phys.* **81**, 253
Schmieder, B., Malherbe, J.M., Mein, P., Tandberg-Hanssen, E.: 1984, *Astron. Astrophys.* **136**, 81
Schmieder, B., Raadu, M., Démoulin, P., Dere, K.P.: 1989, *Astron. Astrophys.* **213**, 402
Schmieder, B., Raadu, M., Démoulin, P., Dere, K.P., Alissandrakis, C.E.: 1990, *Adv. Space Res.* **10**, No. 9, 195